Landslides (2014) 11:67–80
DOI 10.1007/s10346-012-0368-y
Received: 7 August 2012
Accepted: 31 October 2012
Published online: 14 November 2012

E. M. R. Paguican · B. van Wyk de Vries · A. Lagmay

Hummocks: how they form and how they evolve in rockslide-debris avalanches

Abstract Hummocks are topographic features of large landslides and rockslide-debris avalanches common in volcanic settings. We use scaled analog models to study hummock formation and explore their importance in understanding landslide kinematics and dynamics. The models are designed to replicate large-scale volcanic collapses but are relevant also to non-volcanic settings. We characterize hummocks in terms of their evolution, spatial distribution, and internal structure from slide initiation to final arrest. Hummocks initially form by extensional faulting as a landslide begins to move. During motion, individual large blocks develop and spread, creating an initial distribution, with small hummocks at the landslide front and larger ones at the back. As the mass spreads, hummocks can get wider but may decrease in height, break up, or merge to form bigger and long anticlinal hummocks when confined. Hummock size depends on their position in the initial mass, modified by subsequent breakup or coalescence. A hummock has normal faults that flatten into low-angle detachments and merge with a basal shear zone. In areas of transverse movement within a landslide, elongate hummocks develop between strike–slip flower structures. All the model structures are consistent with field observations and suggest a general brittle-slide emplacement for most landslide avalanches. Absence of hummocks and fault-like features in the deposit may imply a more fluidal flow of emplacement or very low cohesion of lithologies. Hummocks can be used as kinematic indicators to indicate landslide evolution and reconstruct initial failures and provide a framework with which to study emplacement dynamics.

Keywords Hummocks · Avalanche · Large landslides · Analog modeling · Horst and graben structures

Introduction

Hummocks are morphological features seen as mounds and ridges that characterize large landslides and debris avalanches. Hummocks are seen on most sub-aerial and sub-marine mass movements on the Earth and also on other planets. They are especially common on volcanic mass movements, for example, the Iriga debris avalanches (Fig. 1) (Voight et al. 1981; Siebert 1984; Glicken 1986). The hummock family includes torevas, which are large tilted and rotated blocks left within or at the foot of the failure scar. Torevas can reach up to several kilometers in size and can disaggregate on their downhill sides into smaller hummocks (Lucchitta 1979; Francis et al. 1985; Wadge et al. 1995). Often steep-sided in the downslope direction, the proximal sides of torevas are often filled in by post-collapse material (Glicken 1991; Palmer et al. 1991). Downslope of the torevas are smaller hummocks. These can have radial or transverse orientation with respect to the landslide transport direction. This arrangement has been explained to be due to basal shear resistance when hummocks are either slowed and sculpted by adjacent faster moving material parallel to the flow direction (Glicken 1986, 1991), stretched during transport (Dufresne 2009), and compressed by deceleration when an avalanche encounters topographic irregularities (Eppler et al. 1987) or water bodies (Siebert et al. 1995). Their shape has also been attributed to faulting formed as the mass spreads (Shea and van Wyk de Vries 2008), suggesting a link between hummock shape and the spreading kinematics.

Hummocks can thus form from horst and graben structures during lateral spreading of an avalanche (Voight et al. 1981, 1983) or by the separation of individual avalanche blocks rafted in finer-grained material (Glicken 1986, 1996; Crandell 1989). Their height and number density often decrease away from source (Ui 1983; Siebert 1984; Glicken 1986, 1996; Crandell 1989), a fact that has been often explained to be due to progressive disaggregation of debris avalanche blocks (Ui and Glicken 1986; Takarada et al. 1999).

Prominent elongated, sub-parallel alignments hummock trains have been considered to be remnants of longitudinal ridges (Dufresne and Davies 2009). Such longitudinal ridges are probably remnants of hummocks dissected by transport parallel strike–slip faults related to lateral velocity changes (Shea and van Wyk de Vries 2008; Andrade and van Wyk de Vries 2010).

Using analog models, we study the evolution and spatial distribution of hummocks in large-scale volcanic landslides. Internal and surface structures and morphology of the mass movements are characterized with the aim to understand the formation and geometry of hummocks and to explore their use as an indicator of landslide kinematics and dynamics.

Methodology

Analog models

Most avalanche analog or numerical model studies have focused on understanding the transport and emplacement mechanisms of landslides (Campbell 1989; Campbell et al. 1995; Pouliquen and Renaut 1996; Staron et al. 2001; Kelfoun and Druitt 2005) and verifying models of granular flow assumed to operate in such events (Denlinger and Iverson 2001; Iverson and Denlinger 2001). Recent analog models by Shea and van Wyk de Vries (2008) and Andrade and van Wyk de Vries (2010) explored the kinematics of rockslides by describing the deposit structure and morphology of the upper brittle layer from the early stages of collapse towards the final phase of material runout. These models use either a polished surface to simulate a low basal friction contact or a ductile basal layer to simulate basal ductile deformation. The main mass of the landslide is modeled by a granular sand-and-plaster mix.

In our models, we assume, like Andrade and van Wyk de Vries (2010), a basal ductile layer and a frictional deformation regime of the main body. In the model, there are basically two deformational regimes: simple shear is concentrated in the ductile base and the brittle body stretches or contracts in predominantly pure shear. The analog models record the continuous movement of a low-viscosity basal silicone layer spreading over an unconfined

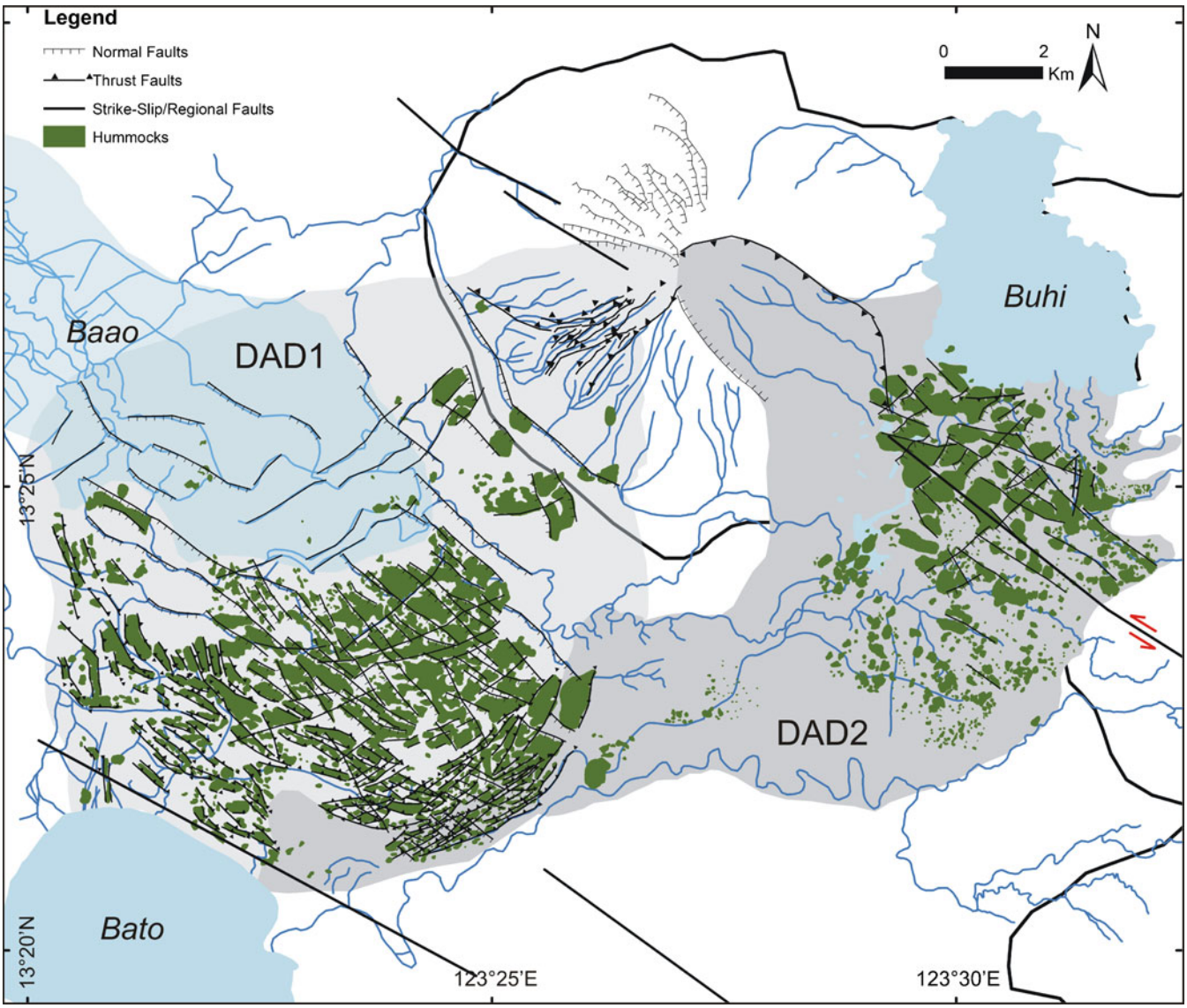

Fig. 1 Iriga Volcano and her two DAD (Paguican 2012; Paguican et al. 2011, 2012) showing the regional faults. Water bodies: Lakes Baao, Buhi and Bato, hummocks. DAD structures—faults and ridges

transport zone. In some models, a lubricating oil layer that simulates a very-low-viscosity basal slide plane underlies the basal viscous silicone layer. These models provide a hybrid between the smooth slide models and the viscous basal models.

Model setup and parameters

We use as a standard model a volcanic cone made of sand and plaster, silicone, and oil (Fig. 2) as used and scaled, for example, by Delcamp et al. (2008), Andrade and van Wyk de Vries (2010), and Mathieu and van Wyk de Vries (2011). Sand and plaster represent the brittle edifice, silicone is the underlying ductile strata, and oil (when used) is the highly lubricated sliding base. The sand–plaster mix has cohesion and internal friction scaled to be similar to most rocky materials of volcanic slopes. By adding plaster, cohesion is raised as described by Donnadieu and Merle (1998). The silicone layer simulates the low-viscosity basal layer in spreading stratovolcanoes and flank collapses (van Wyk de Vries and Francis 1997; van Wyk de Vries et al. 2000; Wooller et al. 2004; Cecci et al. 2005; Andrade and van Wyk de Vries 2010). This layer often consists of mobilized sediments, volcanoclastic, and altered rocks. The oil placed under the silicone in some experiments decreases friction between the sliding basal layer and the plastic sheet, thus speeding up sliding. In such cases, simple shear is concentrated in the oil layer and the rest deforms by pure shear stretching. This layer represents a possibly very-low-resistance layer that could be present at an avalanche base (e.g., Thompson et al. 2010; Siebert 1984).

The failure angle of the landslide (i.e., its initial plan shape) and inclination of transport and depositional areas are also taken into account in the analog models (see Table 1 for the scaling variables). Failure occurs in the edifice when the basal layer deformation induced by the cone load and pressure gradient creates stresses greater than the strength of the sand or sand and plaster. The collapsing material then slides and spreads downslope on a plastic-covered table that can be inclined up to 10°. In each model

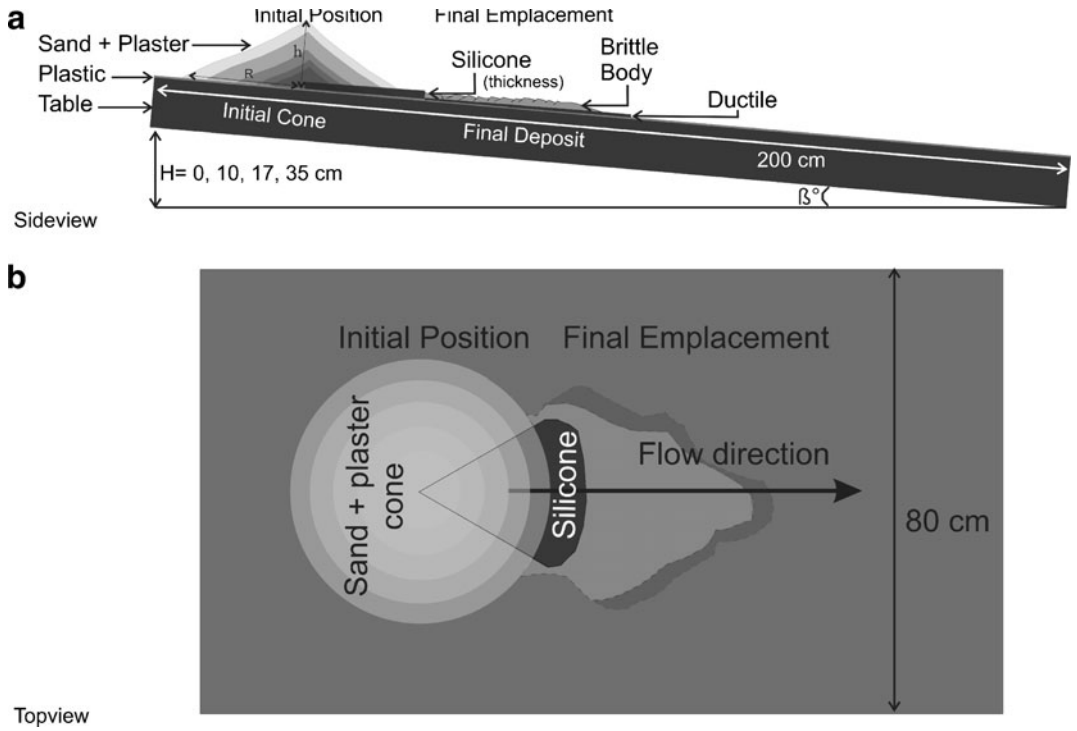

Fig. 2 Analog model setup and illustration of geometrical parameters in **a** vertical view and **b** plan view. Constants and scaling parameter values are given in Tables 1 and 2

experiment, initiation and deposition slopes are fixed at 0°, 3°, 5°, or 10°.

Three sets of experiments were made. Set 1 used pure sand of negligible cohesion (~0 Pa) with oil under 1 or 2 cm of silicone (see Table 2 for dimensionless ratios). Set 2 used different cohesion granular layers with sand and plaster proportions of: 3:1 (250 Pa); 1:1 (500 Pa), and 1:3 (750 Pa) and has oil under 1–2 cm of silicone. Set 3 has the same ratio of cone material as in set 2 but underlain by 1 cm of silicone without lubrication. In some of the experiments, model cones are topped with pure plaster to enhance the visibility of structures formed after collapse.

In total, 45 experiments were completed. There were nine experiments for set 1, 24 for set 2, and 12 for set 3. Sequential photographs (plan view) were taken to record the development of surface structures. Vertical sections were made for the set 1 experiment to view internal deformation within the landslide field. Repetition of the same experiments with identical initial parameters showed the same geometric, morphologic, and dynamic characteristics, thus demonstrating reproducibility.

Scaling

The scaling procedure used in the analog experiments is the same as in previous models that simulate flank destabilization and catastrophic volcano collapses (Donnadieu and Merle 1998; Lagmay et al. 2000; Vidal and Merle 2000; Andrade and van Wyk de Vries 2010). Geometric, kinematic, and dynamic scaling between the analog experiment and real stratovolcanoes is calculated based on the parameters listed in Table 1.

Scaling determines the conditions necessary for proportional correspondence between geometric features and forces acting in nature and in the laboratory. According to the Buckingham Pi theorem, ten independent dimensionless variables must be defined and need to be similar between models and nature. Five of the variables are geometrically and closely similar (defined in Table 2). Five kinematic and dynamic variables are calculated using the gravitational (F_G), inertial (F_I), failure resistance (F_R), and viscous (F_V) forces acting on both natural and analog models, which are defined as:

(1) $F_G = \rho \times g \times h$
(2) $F_I = \rho \times V^2$, where V is the process velocity
(3) $F_V = \frac{\mu}{t}$, where t is the process time
(4) $F_R = C + \frac{h}{R}\left(2\frac{F_G}{3} - F_V\right)$, C is the edifice cohesion and R is the edifice radius, assuming a Navier–Coulomb failure.

The densities of sand layers comprising the model cone layers were similar and averaged at 1,500 kgm^{-3}. Our scaling procedure considers the difference in the average bulk density of a volcanic edifice estimated at 2,200 kgm^{-3} (Williams et al. 1987), and a basal pumice-rich ignimbrite or sediment with densities in the range of 1,400 to 2,100 kgm^{-3} (Bell 2000).

The heights of the analog cones are (1 cm=0.12 km in nature) 12, 11, and 11–15 cm for set 1, 2, and 3 experiments, respectively. Each one is built with slopes of 25–30°, the angle of repose of stratocones. The model cones for set 1 and 3 experiments have a radius of 15 cm and for set 2 was 16 to 17.5 cm. Each model is scaled with respect to the radius of the Socompa and Mombacho volcanoes that are both gravitational spreading volcanoes with major landslides with their basal perimeters defined by breaks in slope and associated thrust-fold belts (van Wyk de Vries and Francis 1997; van Wyk de Vries et al. 2001).

Table 1 List of scaling variables

Definition	Variable	Unit	Nature (N)	Model (M)	Ratio (M/N)
Edifice height	h	m	1,300	0.11	8.5×10^{-5}
Edifice radius	R	m	4,000	0.15	3.8×10^{-5}
Edifice cohesion	C	Pa	10^4	250	0.025×10^{-5}
Edifice density	ρ	kg m^{-3}	2,200	1,500	0.7
Basal layer angle	α	rad	p	$p/6$	0.17
Basal layer length	D	m	8,000	0.18	2.3×10^{-5}
Basal layer vertex distance	d	m	?	0	–
Basal layer thickness	T	m	200	0.01	5×10^{-5}
Basal layer viscosity	μ	Pa s	10^7	20,000	0.002
Basal layer density	γ	kg m^{-3}	1,400	1,000	0.7
Failure and deposition slope	β	°	0–45°	0°, 3°, 5°	0–0.1°
Velocity	V	m s^{-1}	100	10^{-6}	10^{-7}
Time	t	t	60	>3,600	>60
Gravity acceleration	g	m s^{-2}	9.8	9.8	1

The low-viscosity ductile basal layer of the analog models is composed of equilateral silicone pieces, 18 cm in length, and has a varying thickness of about 15 % of the model cone height. The vertex of the silicone is always placed at the center of the cone to ensure that edifice collapse includes the summit. The edges of the silicone define the lateral limits of the subsequent collapse amphitheater.

Sand and plaster cohesion were scaled to the cohesion of volcanic rocks that range from 10^6 to 10^8 Pa for intact basalts and other lavas, 10^2 to 10^5 Pa for volcanic ash and tephra (Afrouz 1992; Bell 2000), and 10^4 to 10^7 Pa for both lavas and tephra. There is no direct measurement for the basal layer viscosity during catastrophic collapses, but it may be estimated in the order of 10^7 Pa s from numerical

Table 2 Definition and values of the independent dimensionless variables (after Andrade and van Wyk de Vries (2010))

Dimensionless variable	Definition	Equation	Value						
			Nature	Model (M1)	Model (M2)	Model (M3)	$\frac{M_1}{N}$	$\frac{M_2}{N}$	$\frac{M_3}{N}$
π_1	Edifice (height/radius)	$\frac{h}{R}$	0.3	0.7	0.7–0.9	0.8	~1	~1	~1
π_2	Basal layer thickness/edifice height	$\frac{T}{h}$	0.1–0.2	0.1–0.2	0.1	0.1–0.2	~1	~1	~1
π_3	Basal layer length/edifice radius	$\frac{D}{R}$	1.3–2	1.2	1–1.1	1.2	~1	~1	~1
π_4	Basal layer vertex distance/edifice radius	$\frac{d}{R}$	?	0	0	0	–	–	–
π_5	a, angular distance	$\frac{\alpha R}{h}$	1.6–10.8	0.7	0.6–0.8	0.7	~1	~1	~1
π_6	Edifice/basal layer density	$\frac{\rho}{\gamma}$	1–1.6	1.5	1.5	1.5	~1	~1	~1
π_7	Gravitational/viscous forces	$\frac{F_G}{F_V}$	168–375	291	291–397	317	~1	~1	~1
π_8	Frictional/viscous forces	$\frac{F_R}{F_V}$	32–36	186–276	178–361	168	~1	~1	~1
π_9	Inertial/viscous forces	$\frac{F_I}{F_V}$	1.3–132	3×10^{-4} -3×10^{-5}	3×10^{-4} -3×10^{-5}	3×10^{-4} -3×10^{-5}	Low	Low	Low
π_{10}	Inertial/gravity forces	$\frac{F_I}{F_G}$	0.8–0.00352	9×10^{-7} -9×10^{-8}	9×10^{-7} -7×10^{-8}	8×10^{-7}–8×10^{-8}	Low	Low	Low

analysis and simulations of debris avalanche flows (Sousa and Voight 1995; Dade and Huppert 1998; Kelfoun and Druitt 2005; Andrade and van Wyk de Vries 2010). The analog silicone has a viscosity of ~10^4 Pa s and the oil ~10^{-1} Pa s.

Results

Standard experiment

The experiments generally result in shorter runout than in the natural counterpart as at a late stage deformation becomes very slow; however, the morphology and structures observed are similar to those observed in large-scale landslide deposits and are seen to remain similar in those experiments that attained scaled natural runouts (Fig. 1; Online Resource 1). Despite changing variables and configurations in the sets of experiments, there are recurrent morphological features and structures that are developed across the experiments. The structures produced are thus general features, and their appearance does not depend strongly on thickness of silicone or cohesion of the brittle layer.

Deformation of the analog cones starts as soon as they are constructed and ends when deformation is almost negligible and overall morphology remains invariable. The rates of deformation depend mainly on the silicon viscosity, the presence of an oil layer, and to a lesser extent on the sand–plaster mixture cohesion. Experiments that have long runout are stopped when the analog landslide reaches the end of the table setup.

Model avalanche class

Model avalanches can be of three classes and can develop three types of hummock morphology and structure (Fig. 3; Online Resource 1): class A avalanches have progressive spreading and extension, class B avalanches undergo progressive spreading but have a localized early compression phase related to the spreading proximal zone pushing against a decelerating distal area, and class C avalanches have late-stage compression in the deposition zone. Individual avalanches can change from one type to another during their development.

Surface morphology and structures

There are two major zones identified in our experiments (Figs. 3, 4, and 5): the collapse zone, which is equivalent to the toreva domain of Andrade and van Wyk de Vries (2010), and the depositional zone, formed when the avalanche progresses out of the amphitheater limits, laterally and longitudinally spreading out material at its base. These two zones are generally separated by a major graben that Andrade and van Wyk de Vries (2010) also observed. This graben is an arcuate depression perpendicular to the slide direction. It separates the area of larger toreva-like hummocks from the zone with smaller hummocks (Figs. 3, 4, and 5).

The collapse zone is further sub-divided into the upper, the middle, and the lower collapse areas (Fig. 3). The upper collapse area is composed primarily of summit material dominated by normal faults oriented perpendicular to the slide direction; the middle collapse area is where numerous strike–slip faults appear; and the lower collapse zone is where arcuate normal faults, with convex traces towards the volcanic cone, are dominant. Irregularities of elevation profile in the collapse zone are due to toreva tilting and rotation.

The depositional zone is sub-divided into the proximal, medial, and distal areas. It is where torevas and blocks break up as the landslide spreads laterally and longitudinally. Prominent features in this zone are lateral levees, ridges, and hummocks (Fig. 3). The depositional zone, like the collapse zone, is cut by normal, strike–slip, and thrust faults. Normal faults appear in extension-dominated areas, where they accommodate basal shearing, tilting, and rotation of the sliding materials. They also appear in the medial to distal depositional zones as the deposits spread further. Thrust faults dominate in the proximal and distal accumulation zones where the materials approach gentler slopes or at the frontal edge where margins resist spreading. Arcuate transtensional faults form in the sliding direction because of the differential forward movement of the deposit combined with lateral spreading.

Hummocks and torevas are observed in all experiments (Fig. 3). Large hummock trains in set 2 and 3 experiments are parallel to the slide direction. In set 1, they are transverse and curved towards the frontal margins. For sets 2 and 3 with 1:1 ratio of sand and plaster, both large and small hummocks form and are superimposed on the same area. Large hummocks are elongated, whereas the smaller hummocks are equant. Only small and rounded hummocks are observed in experiments with the less cohesive, pure sand set 1 experiments.

Plan view shape

Avalanche deposits produced in set 1 and 2 experiments with oil have long runout equaling that of natural deposits, whereas set 3 without the oil have a short runout and with a wide depositional zone (Figs. 3 and 8). The presence of the oil layer and low cohesion of the cone edifice in the experiments influences the landslide runout shape and length (exp. 1.6, 2.3, and 2.7 in Fig. 3). On the other hand, the absence of oil and higher cohesion dampens spreading of the avalanche front. There is instead enhanced lateral spreading that generates a wide depositional zone (exp. 3.6 and 3.8 in Fig. 3). Lobes can form at the frontal and lateral ends of each landslide deposit, and the lobe shape can vary (Fig. 3). Experiments with oil produce landslide deposits with irregular lobes. Those without lubrication have symmetrical, more rounded, and more regular lobes. This is attributed to the presence of oil layer as the reduced friction by lubrication of the silicone affects the basal- and upper-layer spreading rate on both lateral and frontal margins.

Subsurface deformation

Vertical cross-sections (Fig. 5a), parallel to the main sliding direction, reveal the avalanche internal structure. The collapse and depositional zones are dissected by normal faults and are separated by a graben. Strike–slip faults, often trending arcuate towards the frontal margin, are difficult to see in this view but are clear in the plan views in Fig. 3. In the collapse zone, listric normal faults converge into the ductile shear zone. The listric normal faults accommodate the sliding, tilting, and rotation of the blocks in the collapse zone.

In the depositional zone, the listric faults are more shallowly dipping and more closely spaced. In the topmost part of the brittle distal layer, there are also shallower and minor low-angle normal faults that accommodate the sliding, tilting, and rotation of smaller blocks within the brittle material. These produce the

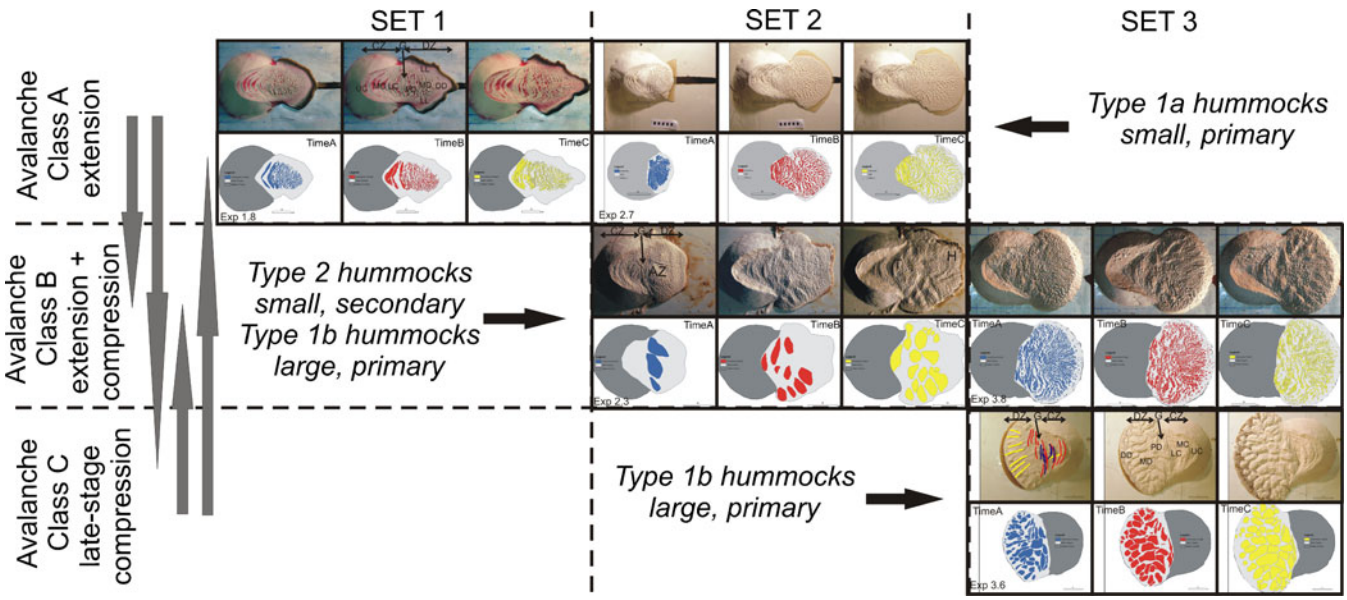

Fig. 3 Development of analog avalanches. Five analog models that represent the three sets of experiments are grouped according to avalanche classes and the resulting hummock types: one for set 1 and two each for sets 2 and 3. Avalanches can be of class A with progressive spreading and extension resulting in progressively broken, primary, smaller hummocks, Hummock type 1a; avalanche class B for progressive spreading with internal compression in some areas resulting in a wider range of hummock size. Hummock type 1b and 2 or avalanche class C for progressive sliding with late-stage compression resulting in increasing hummock size. Hummock type 1b. *Gray arrows* indicate that during an avalanche, hummocks can start big and break during extension or they can merge sometime during their development. For each experiment, three photos representing the avalanche evolution and hummock development are presented in the first row, with their hummocks, debris field, and depositional zone delineations below for statistical analysis of hummock area and spatial distribution. Morphological features are labeled and delineated in some experiments: collapse zone (*CZ*) and its upper (*UC*), medial (*MC*) and lower (*LC*) areas; depositional zone (*DZ*) and its proximal (*PD*), medial (*MD*), and distal (*DD*) areas; the graben (*G*); accumulation zone (*AZ*) in the PD, MD, or DD, ridges (*R*), torevas (*T*), and hummocks (*H*); and the surface structures: normal (*red*), thrust (*blue*), and strike–slip (*yellow*) faults

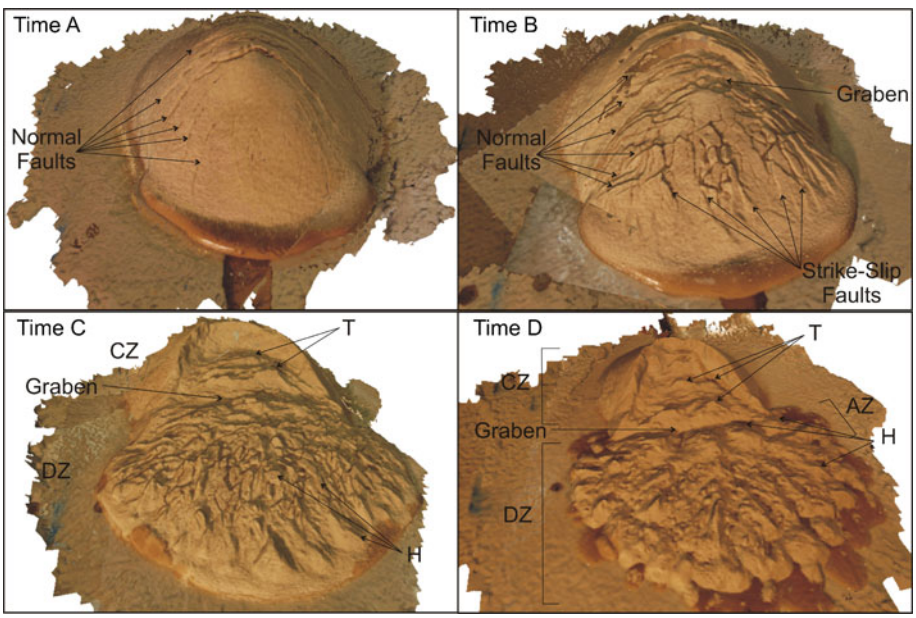

Fig. 4 A 3D visualization example of structural and morphological development of an avalanche and formation of hummocks during its evolution (the 3D models are created by the ARC 3D webservice, developed by the VISICS research group of the K.U. Leuven in Belgium). Time A, formation of normal faults and movement along these cause edifice extension downwards by sliding; time B, collapse of more edifice materials near the summit and formation of more normal faults in the collapse (*CZ*) and depositional (*DZ*) zones. Movement along these faults spreads the materials further down, with the graben forming as the edifice materials come out of the amphitheater limits towards a gentler slope. At time C, torevas (*T*) formed since the earlier stages are more evident and the materials at the base spread both to the lateral and downslope directions. Hummocks in the DZ are well formed at this stage, and at time D, the avalanche spreads and hummocks break up

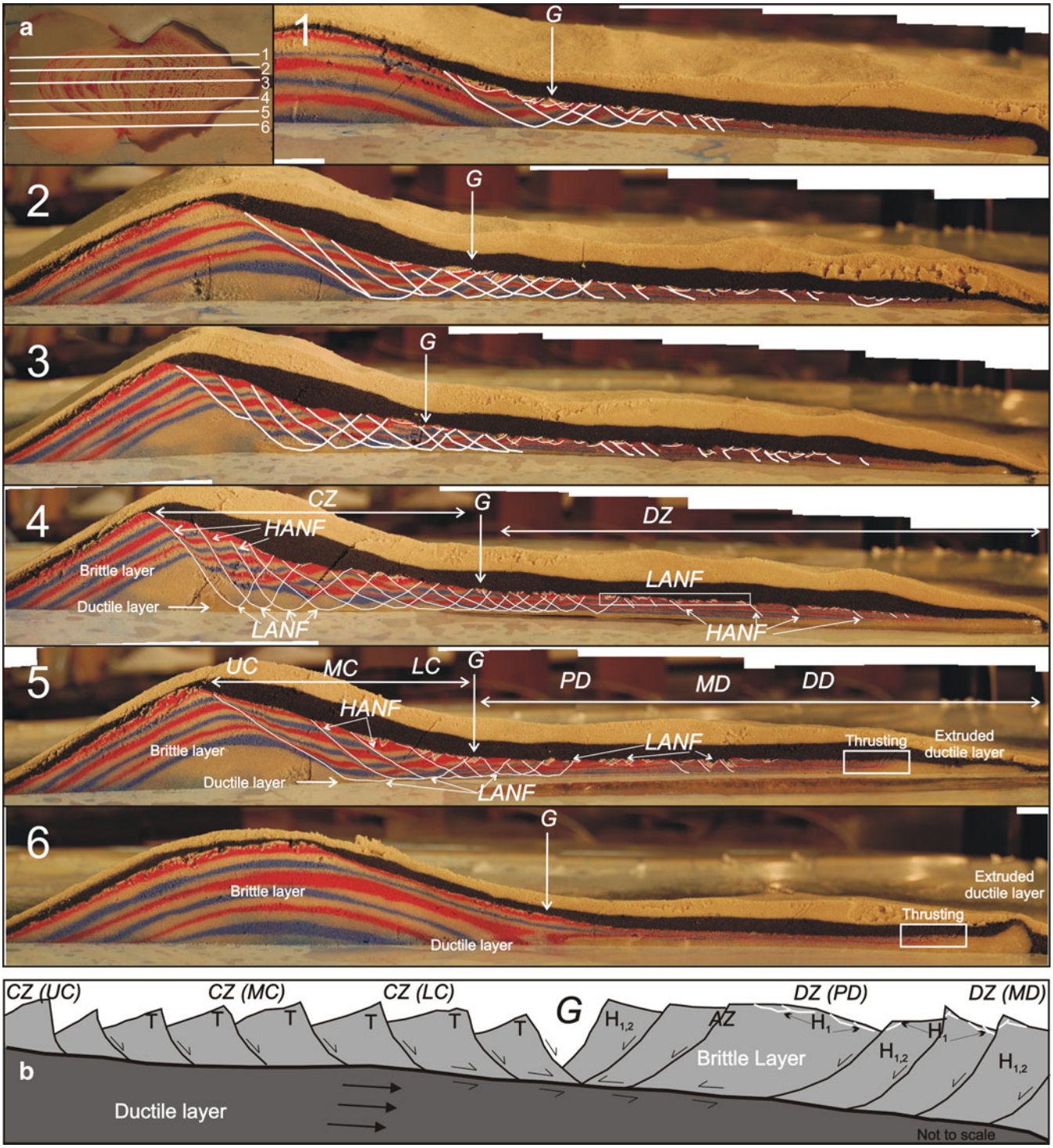

Fig. 5 Sub-surface (**a**) vertical view parallel to slide direction of an analog avalanche and (**b**) interpretation. **a** Plan view image for the locations of the cross-sections *1–6*. The different sub-areas for collapse and depositional zones and graben are shown in *1–6*. The analog has an upper brittle layer where normal faults are evident and a ductile layer underneath with varying thickness throughout the avalanche area. High-angle normal faults (*HANF*) in the upper brittle layer become listric and converge into a low-angle normal fault (*LANF*). These faults accommodate the sliding, tilting, and rotation of edifice blocks in the collapse zone, forming the torevas and their smaller counterpart, first-order type 1 and second-order type 2 hummocks. On the topmost part of the brittle layer are shallower low-angle normal faults that accommodate the sliding, tilting, and rotation of minor blocks at the very top, forming the type 2 hummocks. **b** A cross-section interpretation of an avalanche

secondary small hummocks that appear like detachment blocks gliding on top of the deposit or sometimes stranded on top of the larger hummocks.

The graben is a transition point of the normal faults between the collapse and depositional zones. It is where sliding torevas start to break up as the landslide spreads into a wider depositional

zone or where torevas accumulate as they approach a gentler slope.

In general, the dip of normal faults decreases with depth and distance from the summit. This is shown by listric faults that converge in the boundary of the upper brittle layer and the underlying ductile layer in the collapse zone. Many shallow normal faults do not reach this boundary in the depositional zone but flatten into the lower part of the brittle material. The high- and low-angle normal faults in the collapse zone create the torevas. In the depositional zone, they create hummocks. Figure 5b shows a cross-sectional interpretation and morphology of these structures.

From the collapse zone towards the proximal deposition zone, brittle shearing dominates as ductile shearing only occurs in the upper part of the thinning silicone. From the medial towards the distal deposition zone, however, ductile shearing dominates, resulting in both the thrusting of the silicone and thinning or thickening of the sand–plaster layer.

Hummocks

In this study, each experiment is divided into three stages: initial, development, and final deposition. Experiments that best represent the recurrent morphology and structures are chosen and presented in Fig. 3 and Supplement A. Using statistical analysis, hummock area, spatial distribution, and factors affecting it are explored for patterns that aid to investigate their types and evolution throughout the landslide–avalanche development.

Characterization

We distinguish two types of hummocks formed in the experiments (Figs. 3 and 5): type 1—primary hummocks and type 2—secondary hummocks. Type 1 hummocks are of two classes: type 1a are the small and generally equant hummocks formed early on through the initial development stages of faulting and may undergo minor breakup during emplacement and type 1b are formed at the same time but are the larger and often elongated hummocks. Type 2 forms on top and alongside the larger type 1b hummocks. Type 1b hummocks develop from original landslide blocks that became stretched and flattened, and they may also grow from the accretion of other type 1 hummocks.

Exploratory statistics

Hummock area is automatically calculated from registered experiment photographs managed in a GIS. Hummock number density is generated using the center of a hummock and number per unit area. A line graph of increasing hummock area (Fig. 6) shows that experimental avalanches can produce either a highly contrasting or a gradually changing population of hummock type. Small hummocks, types 1a and 2 (exp. 1.8, 2.7, 2.3, 3.8) resulting from class A and B avalanches (extension during avalanche), tend to have a very high frequency of small and very few big hummocks. This is seen by the very abrupt change in slope on Fig. 6. Type 1b hummocks produced by class B and C analog avalanches (with compression at some points during the avalanche) (exp. 2.3, 3.8, 3.6) exhibit gently sloping graphs, indicating that within certain stages during the avalanche the hummocks are of restricted range of sizes. In general, hummock population may decrease as their size increases or populations increase as they progressively break up.

During an avalanche, types 1a and 2 small hummocks break up and disintegrate if they are formed by lower-cohesion material as shown by an overall decrease in hummock size (Fig. 7a; Online Resource 2, left). However, as an avalanche slows or when cone materials block the spreading of silicone at the front of the avalanche causing compression, hummocks can merge and grow (Fig. 7b; Online Resource 2, right). This results in larger hummocks at the medial to distal margins.

Spatial distribution

Hummock spatial distribution is recorded using the center of each hummock as described in Yoshida et al. (2012). The elongation and direction of the ellipse (Fig. 8) represents the general direction and orientation in which all the hummocks form and separate. In general, this ellipse follows the plan view shape of the debris avalanche deposit itself.

The mean center (Fig. 8) shows the point where the hummock population center moves at each stage of the experiment. In general, these trends allow visualization of the link between central hummocks, the overall direction of movement, and the avalanche flow direction. The trend in the directional ellipse and mean center of the hummock areas show that spreading occurs mostly parallel to the long axis of the avalanche for low-cohesion material and with a lubricated base. In contrast, spreading is dominantly lateral for high basal friction and more cohesive experiments.

Sequence of events

The development of a rockslide debris avalanche model can be sub-divided into three stages depending on the structures and morphological features that form. These are the slide initiation, development, and final emplacement. The slide initiation stage is also described by Andrade and van Wyk de Vries (2010), but they did not carry the models further. A discussion regarding these stages is presented in this section with accompanying diagrams (Figs. 4 and 9) that show the development of the overall morphological and structural features and the formation and evolution of hummocks.

Slide initiation

Fractures begin to develop at the onset of edifice collapse. As soon as the underlying ductile layer in the experiments begins to stretch, sliding initiates and transforms early fractures into faults. These faults define the amphitheater walls (Figs. 4a and 9) and also accommodate the extension of edifice blocks as the landslide–avalanche spreads outwards. These blocks may become torevas if they remain intact in the collapse zone or the proximal area of the depositional zone. If broken into smaller blocks, they become type 1 hummocks in the depositional zone. Transtensional faults in the collapse zone start to appear early on.

Development stage

The collapse, depositional zones, and horst and graben structures become obvious during the development stage (Figs. 4b, c and 9). More normal faults form and edifice materials slide in both zones. Large blocks and torevas at the lower part spread more, break up, and form the smaller hummocks (Type 1a, 2). Some torevas remain intact and some can accumulate and combine with neighboring ones, forming the larger type 1b hummocks.

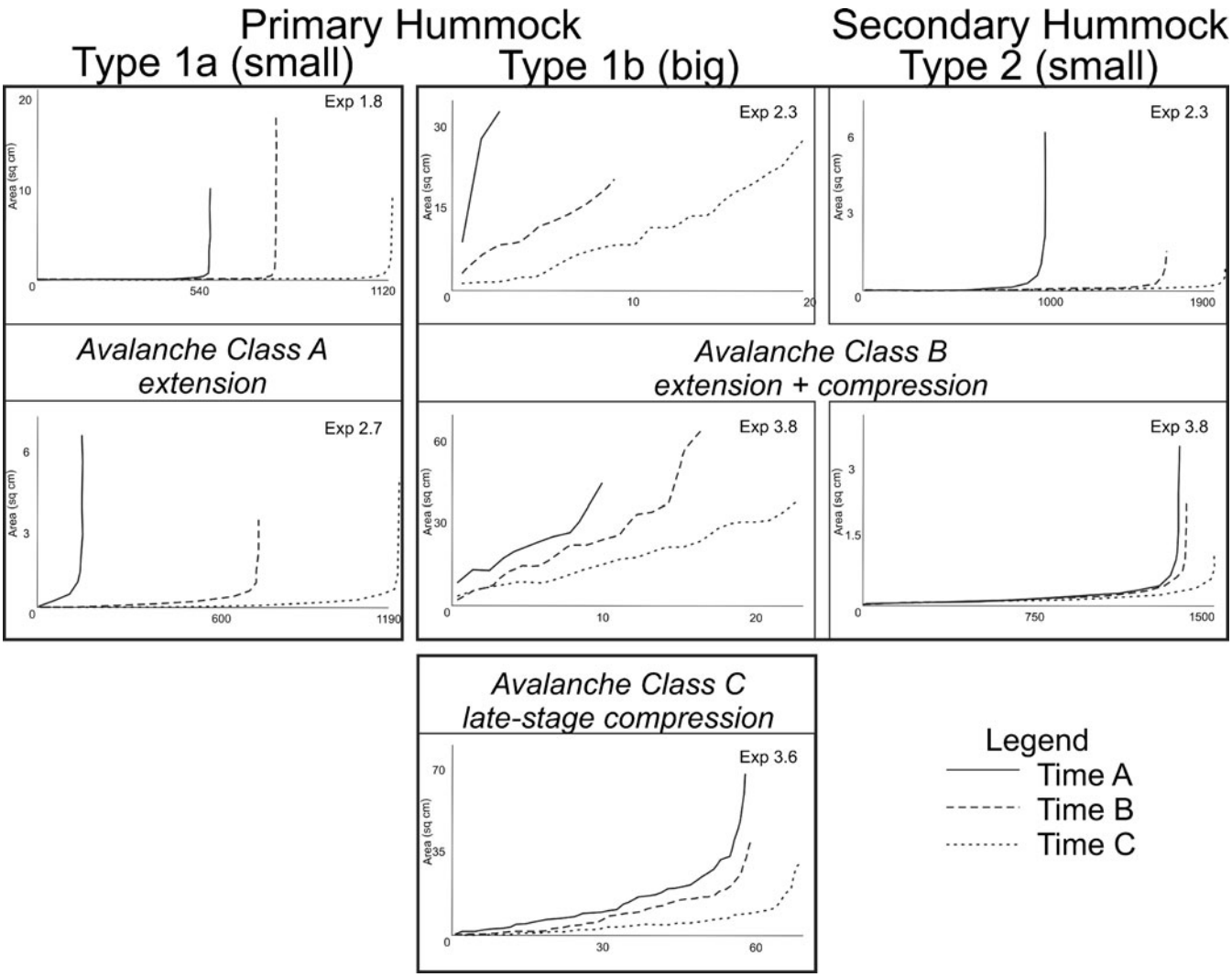

Fig. 6 Increasing line plot of hummock area. Avalanches can produce either a combination of a large number of small hummocks or a very low count of big hummocks. Small hummocks, regardless of whether they are primary or secondary, can be highly contrasting, having mostly very small and very few large hummocks. Sizes of type 2 hummocks, however, exhibit a gradual change in slope, implying that for avalanches that produce larger hummocks (compression-dominated avalanches), their hummocks are of similar sizes during transport

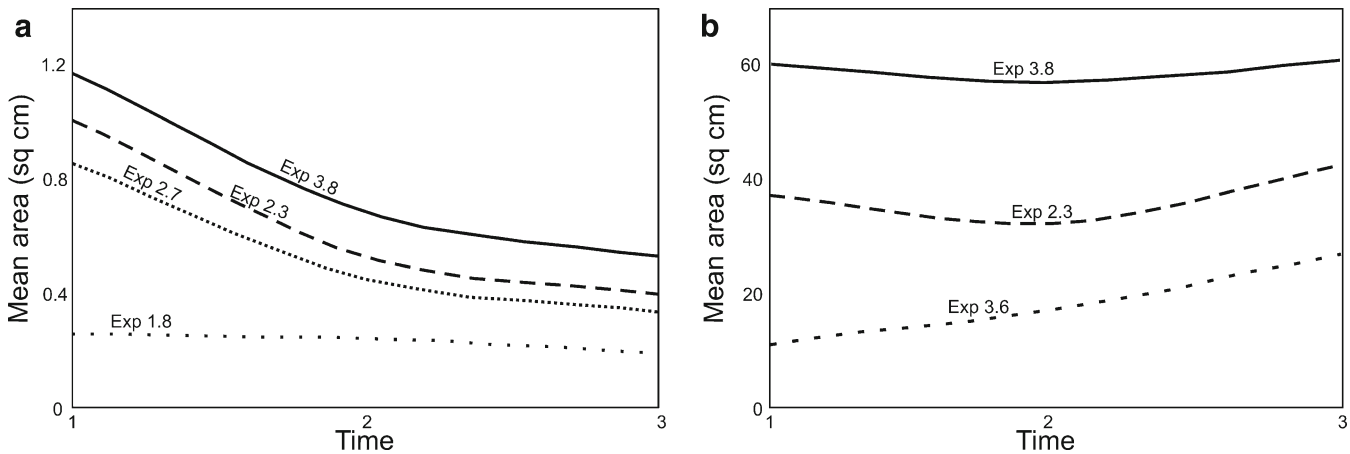

Fig. 7 Line graph showing the mean areas of hummocks with respect to the distance from the summit (the greater the time, the farther the hummocks are from the source). Type 1 (**a**) and type 2 (**b**) hummocks will always tend to break up due to spreading and extension during an avalanche emplacement. However, they can start to merge and form together with an increase in size once they undergo compression

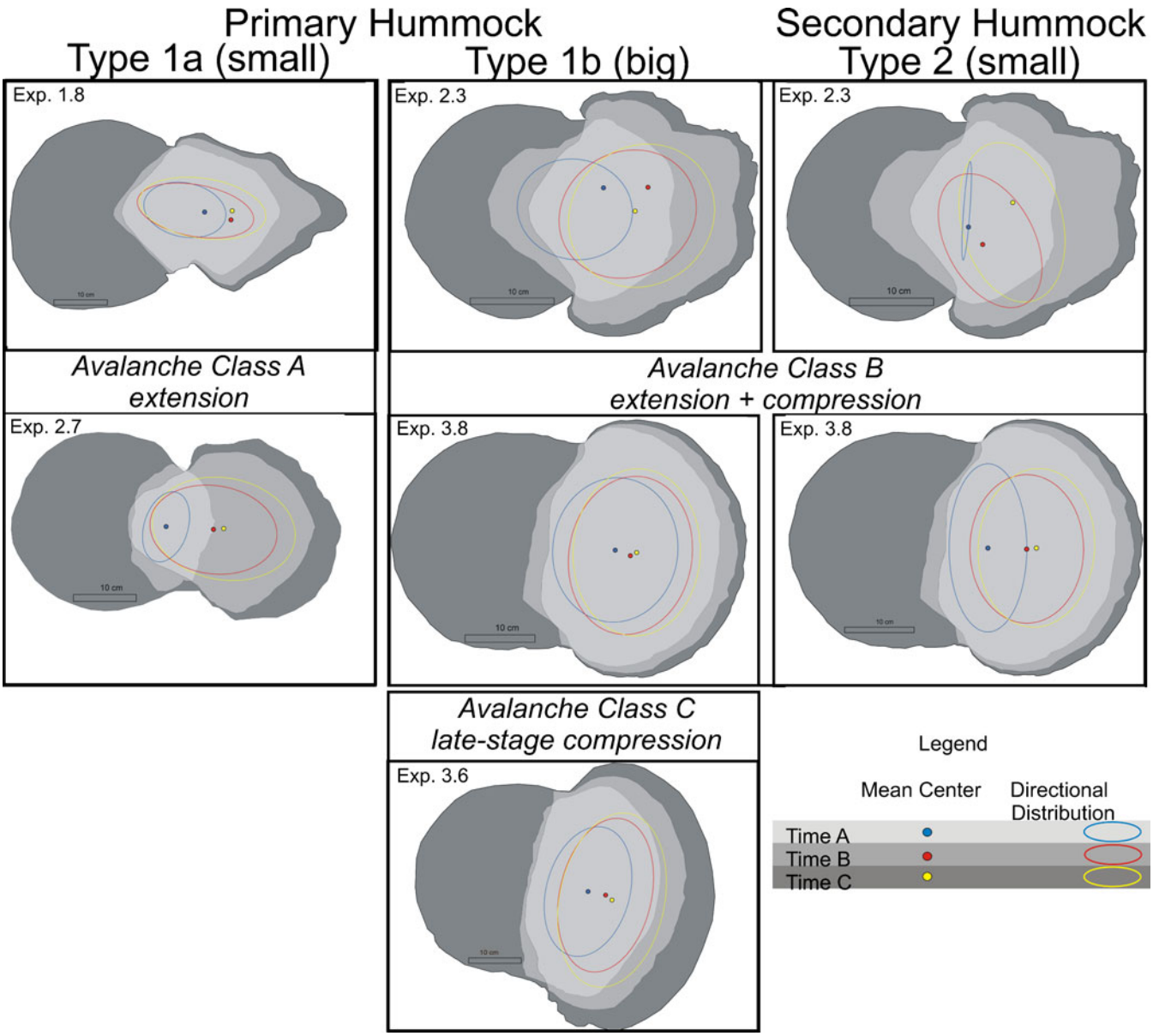

Fig. 8 Trend of the directional ellipses and mean centers. The directional ellipses show the lateral or longitudinal formation direction of hummocks and the mean center is the center point of the central hummock

Final stage

During the final stage, type 2 detachment hummocks become evident, whereas torevas in the collapse zone remain unchanged. In the depositional zone, hummocks can break up or remain intact as the avalanche continues to spread. The ductile layer may build up at the margin where a thrusted brittle upper layer forms compression ridges.

Discussion

To understand what hummocks are and how they are formed, their relationship with other structural and morphological features within an avalanche field must first be recognized. From the analog models, we observe that hummocks form in all experiments but that their final spatial distribution, size, elongation, and morphology can vary (Fig. 2).

Avalanche characteristics

The analog avalanche models constructed in this study develop a similar and consistent set of structures. In all of the experiments, the collapse and depositional zones are separated by a graben and faults dissect the entire mass (Figs. 3, 4, and 5). In the collapse zone, large listric faults form the main failure planes of the avalanche. From the middle towards the base of the collapse zone, transtensional and compressional faults appear as the collapsing mass spreads outwards (Figs. 3, 4, and 5). The areas between the faults are the hummocks, effectively horsts.

The depositional field has three areas: the proximal, medial, and distal areas. Size, orientation, elongation, and spatial distribution of the hummocks are different in each of these areas and are controlled by varying emplacement conditions.

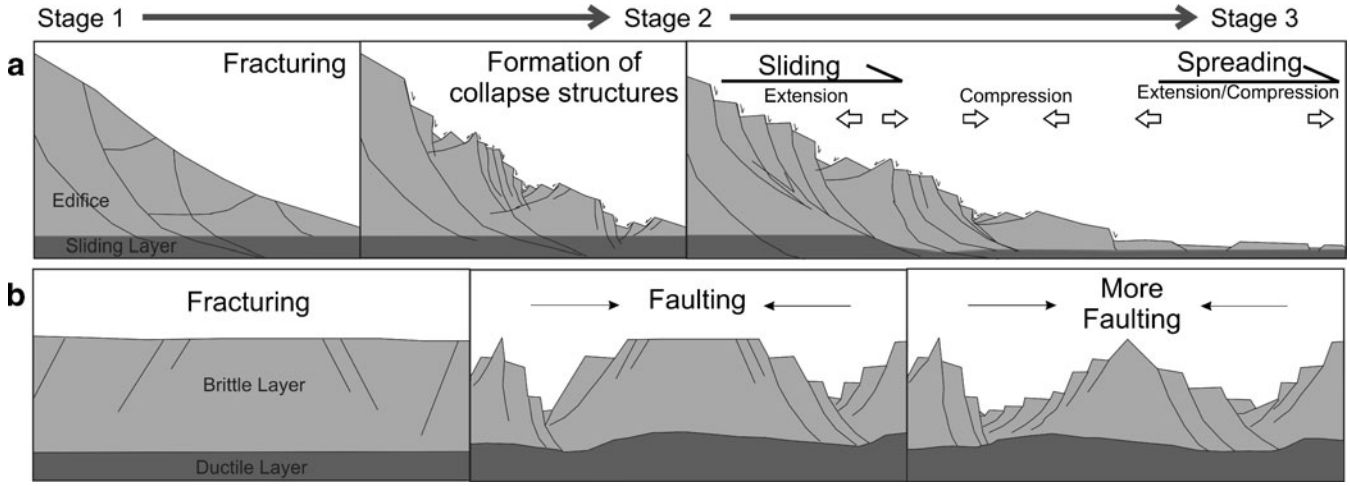

Fig. 9 The different stages of avalanche emplacement showing an interpretation of hummock formation (**a**) and degree of faulting (**b**)

In experiments where a low-cohesion pure sand cone stands on an inclined plane and the base is oil-lubricated, progressive but gradual spreading and thinning of the avalanche is observed (Fig. 3). On the other hand, in more cohesive models of sand and plaster cones on a gently inclined plane, regardless of lubrication at the base (Fig. 3), higher friction and resistance to slide result in an accumulation area within the depositional zone. Hummocks are formed from the broken edifice blocks that slid, tilted, and rotated as the avalanche progresses.

Hummock description

Morphology

Hummocks can be characterized according to their basal shape, surface morphology, and orientation with respect to flow and slide direction. The basal shape of hummocks can be equant, circular, rectangular, or elliptical. Hummock deformation and shape after initial formation depends on the velocity distribution and the strain field of the avalanche. Their initial shapes stretch along acceleration and contract on the deceleration directions. Hummock elongation is a product of initial shape and subsequent deformation that can be either dominantly parallel, perpendicular, or randomly oriented with respect to flow direction. The surface morphology of hummocks can be flat-topped or pointed, ridged, or rounded. Densely faulted hummocks can create pinnacle-topped features (Fig. 9b).

Generally, circular-based and flat-topped hummocks are formed in rapidly emplaced long-runout models, whereas elongated and pinnacle hummocks form in experiments of cohesive avalanche material with moderate runout. The high slope angle of collapse base, lower cohesion, and greater lubrication can increase the runout length and decrease the lateral or longitudinal spreading direction, shape, and orientation of individual hummocks.

Types

We identify different hummock types based on their size and development (Fig. 3): type 1a are the first-order small hummocks; type 1b are the first-order large, elongated hummocks; and type 2 are the second-order small, polygonal hummocks that formed after and raft over the type 1b hummocks. The extensional faulting of avalanche deposits forms the first-order hummocks. Small-scale shear faulting or brittle fracturing separating and detaching the stretched upper layers of the larger primary hummocks forms the type 2 hummocks. They are a boudinage feature of stretched and separated competent layers, such as those seen in many avalanche hummock cuts (e.g., Fig. 5f in Shea et al. (2008) or Fig. 4 in Bernard et al. (2009)) or in other avalanche analog models (Shea and van Wyk de Vries 2008).

From the vertical cross-sections, we observe that high-angle normal faults in the upper brittle layer converge into low-angle normal faults towards the lower part, accommodating the sliding, tilting, and rotation of edifice blocks forming the type 1 hummocks. The shallower low-angle normal faults or brittle fractures on the topmost part of the brittle layer serve as a décollement interface of the different lithologies forming the type 2 hummocks.

Trends in size and spatial distribution

Hummocks can have a low population density with a large size distribution, as is generally the case when type 1b hummocks are present, or there can be a high population but with a small size distribution, as in the case for deposits with dominantly small hummocks (types 1a and 2). If a model avalanche produces large hummocks, the difference in size distribution is minimal. On the other hand, if smaller hummocks form, their size range is broad, with most hummocks at the lower end of the size spectrum.

As an avalanche develops, hummocks can decrease in number but increase in size or they can increase in number but decrease in size. At the final stage, however, hummock population is more often higher compared to the early stages, indicating that hummocks do break up during sliding development.

A progressively spreading and thinning avalanche body (class A) is dominated by extension. The largest hummocks are confined in the lower collapse zone and proximal depositional zone, and type 1a hummocks spread all over the depositional zone. This is observed in Iriga DAD2 (debris avalanche deposit) (Paguican 2012; Paguican et al. 2011, 2012). In avalanche classes B and C where there is substantial compression due to frontal restriction, there are hummock types 1b and 2. The bigger hummocks can be located

anywhere in the depositional zone and can form the accumulation zones. This is clearly observed at the Tetivicha avalanche, Bolivia (Shea and van Wyk de Vries 2008) and Iriga debris avalanche deposits (Paguican 2012; Paguican et al. 2011, 2012).

Avalanche stages and hummock formation

From the analog models, it is clear that hummock formation is intimately linked to the development of the avalanche. At the first stage, normal listric faults accommodate the extension by sliding and rotation of blocks. These blocks are the initial hummocks. Then, during transport, the avalanche may spread freely or may encounter barriers and topographic constraints such as other topography. During this stage, the hummock population develops and evolves.

From landslide to hummocks

The low-angle normal faults at the base and the high-angle normal faults at the upper layer create the sliding plane. This plane facilitates most of the sliding, tilting, and rotation of edifice blocks as the body spreads down the amphitheater. The major normal faults limit the boundaries of the collapse amphitheater. Near the amphitheater base and outside of its limits, edifice materials will start to spread laterally as well as longitudinally. As the sliding plane activates and initiates sliding, brecciation and faulting in the edifice occurs and blocks are formed by the main normal faults. As the collapsing edifice mass moves down, extension of the upper layers above the slide plane induces normal faulting, generating horsts and grabens. The faulted horst blocks become the building blocks of hummocks as the whole mass spreads.

As the edifice materials come out of the amphitheater and into the depositional zone, debris will spread and extend not only downslope but also laterally. As the materials approach the gentler slope at the piedmont, proximal materials accumulate, creating ridges oriented perpendicular to the flow. As more materials slide down from the edifice, these materials are pushed to spread further, where extensional or compressional structures may dominate depending on the topography and morphology of the depositional zone. Naturally, extension happens on unconfined depositional environments with regular topography. On the other hand, compressional features such as ridges parallel, sub-parallel, or perpendicular to the flow direction may develop in confined environments. These ridges may form distal accumulation zones if frontal debris is compressed in the distal front. Distal accumulation zones may be remobilized into lahars if saturated or could remobilize as secondary slides, as at Socompa (Kelfoun et al. 2008; Glicken 1986). High-angle normal faults and tension fractures are not clearly rooted to the basal layer in the depositional zone; their strain is taken up by diffuse deformation in the lower brittle zone or by structures too small to be observed at the model scale.

Spreading and increasing extension by block sliding, tilting, and rotation is the stage when hummocks are developed. As spreading proceeds, hummocks can break and move farther apart, resulting in increased type 1a and 2 hummocks. Conversely, confinement can move hummocks closer and from larger type 1b structures. Figure 4 shows the juxtaposition of type 1b as well as the breakup of the type 1a and 2 hummocks. Such a situation was described at Parinacota (Clavero et al. 2002).

The role of normal faults

The existence of listric normal faults at the collapse zone is a consequence of the geometry of the sliding mass and the brittle and ductile layers present. The main failure plane is the contact where the base of the brittle blocks slides on a non-slip or fused interface with the ductile basal layer or the stable edifice. Relative movements of the blocks are accommodated by pervasive deformation in the ductile layer under this interface. High-angle normal faults in the collapse zone are generally rooted in the basal layer, although this is not the case for those in the shallower depositional zone that do not clearly extend down to the silicone, rather they pass into a lower brittle horizontal stretching area.

Layering within the avalanche, with a sliding or slip layer at the top such as the upper ignimbrite layer or the lower block and ash layer at Iriga DAD2 (Paguican 2012; Paguican et al. 2011, 2012), generates an internal décollement causing minor low-angle normal faulting over the discontinuity. If there is a pre-existing discontinuity between layers allowing the upper layer to glide over the lower layer, this décollement may take up the deformation. Rotational movement of the upper layer could also generate sliding at the interface. These internal avalanche structures exist as a result of layer interfaces that could be caused by a major internal structure or by a contrasting stratigraphy.

Degree of stretching

During the development of the landslide and evolution of hummocks, the scale variation of stretched portions is observed. Post-collapse lengths are mostly twice its pre-collapse basal radii (see Online Resource 1). The width, thickness, and volume of the active area change during stretching. The normal listric faults in the collapse zone decreases in dip as they approach the depositional zone. In the medial to distal areas, they become more horizontal by instantaneous stretching (Fig. 9a).

Based on the increasing degree of stretching (Fig. 9a) and normal faulting (Fig. 9b), the degree of stretching (Fig. 9) changes from stage 1 to 3 (from modified main structural occurrences of stretching in the crust by Brun and Choukroune (1983)). Stage 1 is when the faults begin to form discrete blocks, with more intense deformation between blocks. At stage 2, changes in the thickness of the upper brittle and basal ductile layers begin and are more evident and widely observable in stage 3. Stage 3 is when hummocks are fully formed and tend to spread instead of breaking apart with deformation affecting the surrounding zones. The basal ductile layer becomes thin towards the summit area, and most of it is extruded and spread under the avalanche. The ductile layer may come to the surface due to the high degrees of stretching (the same thing as observed at Socompa (Shea et al. 2008)). Structures shown in the cross-sections (Fig. 5) are those of late stage 4 when the avalanche is nearly fully stretched.

Conclusions

The analog models presented here allow the visualization of the development of landslide–avalanche hummocks and provide a structural and kinematic sequence of their formation. This can then be used to understand natural avalanche hummock structure and distribution and thus obtain the emplacement history. Hummocks are a useful tool for understanding avalanche emplacement.

Hummocks are the morphological expression of brittle layer deformation due to spreading in landslides and avalanches. They are

principally the stretched remains of tilted and rotated blocks of the original failure volume. In general, both landslide–avalanches and hummocks initiate and evolve in a similar way. Landslides and avalanches start with fracturing and faulting of the failure area (or, for a volcano, the edifice). As strain increases, the upper landslide layer can split apart, forming grabens and horsts and creating steeply dipping escarpments parallel to the slide direction. Normal and strike–slip faults accommodate the sliding, tilting, and rotation of blocks that later evolve into hummocks. These faults also accommodate the extension and spreading within hummocks. Therefore, hummocks are formed by extension of the avalanche, with the hummocks spreading and moving apart as the avalanche spreads. They can also move together or compress, or new ridge-like hummocks can form due to avalanche constriction by topography.

The morphology and spatial distribution of hummocks are dependent on the interplay of the number density of normal, thrust, and strike–slip faults, which is a function of strain and material properties such as cohesion and the viscosity of a ductile sliding layer. Hummock shape and size depends primarily on the original position in the initial landslide and the first-formed structures. The hummock shape changes with subsequent spreading, breakup, or merger. During landsliding, hummocks can break up, resulting in a higher number density; on the other hand, hummock merger during compression can reduce number density. At the last stages of emplacement, hummocks can either break or remain intact while spreading farther apart from each other and can spread themselves, increasing their surface area.

The structures within avalanche deposits and hummocks indicate that they form by extension and are consistent with a general slide model where pure shear stretching dominates in the upper brittle part and simple shear is concentrated at the base. When hummocks and fault-like features are not formed, a more fluidal flow type of emplacement could be possible.

Lastly, we call primary hummocks in large landslides and avalanches type 1, which can be divided into two main groups: the type 1a small hummocks, which are generally found toward the front, and the type 1b large hummocks that are initially formed from the initial landslide toreva blocks and are found in the proximal and medial zones. Type 1b hummocks can also form by coalescence during compressive or arrest stages.

The type 2 hummocks are secondary features formed by a boudinage-like process during layer parallel stretching. They can exist on or around the type 1b hummocks and are generally seen as single blocks of more consolidated material.

Avalanches that spread freely (class A) have large numbers of small type 1a and few large type 1b hummocks. Avalanches that become constrained (class B and C) tend to preserve the larger type 1b and tend to have accompanying type 2 secondary ones.

Acknowledgments

This study is a result of the cotutelle Ph.D. program between the Université Blaise Pascal and the University of the Philippines. Funding was provided by the French Embassy in Manila and the EIFFEL Excellence Scholarship.

References

Afrouz AA (1992) Practical handbook of rock mass classification systems and modes of ground failure. CRC, London

Andrade D, van Wyk de Vries B (2010) Structural analysis of the early stages of catastrophic stratovolcano flank-collapse using analogue models. Bull Volcanol 72:771–789. doi:10.1007/s00445-010-0363-x

Bell FG (2000) Engineering properties of soils and rocks, 4th edn. Blackwell, Oxford

Bernard B, van Wyk de Vries B, Leyrit H (2009) Distinguishing volcanic debris avalanche deposits from their reworked products: the Perrier sequence (French Massif Central). Bull Volcanol 71:1041–1056. doi:10.1007/s00445-009-0285-7

Brun J-P, Choukroune P (1983) Normal faulting, block tilting, and décollement in a stretched crust. Tectonics 2(4):345–356

Campbell CS (1989) Self-lubrication for long runout landslides. J Geolog 97:653–665

Campbell CS, Cleary PW, Hopkins MJ (1995) Large-scale landslide simulations: global deformation, velocities and basal friction. J Geophys Res 100:8267–8283. doi:10.1029/94JB00937

Cecci E, van Wyk de Vries B, Lavest J-M (2005) Flank spreading and collapse of weak-cored volcanoes. Bull Volcanol 67:72–91. doi:10.1007/s00445-004-0369-3

Clavero JE, Sparks RSJ, Huppert HE (2002) Geological constraints on the emplacement mechanism of the Parinacota avalanche, northern Chile. Bull Volcanol 64:40–54

Crandell DR (1989) Gigantic debris avalanche of Pleistocene age from ancestral Mount Shasta Volcano, California, and debris-avalanche hazard zonation. US Geolog Survey Bull 1861:31

Dade WB, Huppert HE (1998) Long run-out rockfalls. Geology 26:803–806

Delcamp A, van Wyk de Vries B, James MR (2008) The influence of edifice slope and substrata on volcano spreading. J Volcanol Geotherm Res 177(4):925-943. http://dx.doi.org/10.1016/j.jvolgeores.2008.07.014

Denlinger RP, Iverson RM (2001) Flow of variably fluidized granular masses across three-dimensional terrain. 2. Numerical predictions and experimental tests. J Geophys Res 106(B1):553–566. doi:10.1029/2000JB900330

Donnadieu F, Merle O (1998) Experiments on the indentation process during cryptodome intrusions: new insights into Mount St. Helens deformation. Geology 26:79–82

Dufresne A (2009) The influence of runout path material on rock and debris avalanches: field evidence and analogue modeling. Dissertation, Canterbury University, Canterbury

Dufresne A, Davies TR (2009) Longitudinal ridges in mass movement deposits. Geomorphology 105:171–181

Eppler DB, Fink J, Fletcher R (1987) Rheologic properties and kinematics of emplacement of the Chaos Jumbles rockfall avalanche, Lassen Volcanic National Park, California. J Geophys Res 92:3623–3633

Francis PW, Gardeweg M, Ramirez CF, Rothery DA (1985) Catastrophic debris avalanche deposit of Socompa volcano, northern Chile. Geology 13:600–603

Glicken H (1986) Rockslide debris-avalanche of May 18, 1980, Mount St. Helens volcano. Dissertation, University of California, Santa Barbara

Glicken H (1991) Sedimentary architecture of large volcanic-debris avalanches. In: Fisher RV, Smith GA (eds) Sedimentation in volcanic settings. SEPM Special Publication 45: pp 99-106

Glicken H (1996) Rockslide-debris avalanche of May 18, 1980, Mount St. Helens Volcano, Washington. US Geol Surv Open-File Rep 96–0677:1–90

Iverson RM, Denlinger RP (2001) Flow of variably fluidized granular masses across three-dimensional terrain. 1. Coulomb mixture theory. J Geophys Res 106(B1):537–552. doi:10.1029/2000JB003758

Kelfoun K, Druitt T (2005) Numerical modeling of the emplacement of Socompa rock avalanche, Chile. J Geophys Res 110:B12202. doi:10.1029/2005JB003758

Kelfoun K, Druitt T, van Wyk de Vries B, Guilbaud M-N (2008) Topographic reflection of the Socompa debris avalanche, Chile. Bull Volcanol 70:1169–1187. doi:10.1007/s00445-008-0201-6

Lagmay AMF, van Wyk de Vries B, Kerle N, Pyle DM (2000) Volcano instability induced by strike–slip faulting. Bull Volcanol 62:331–346. doi:10.1007/s004450000103

Lucchitta BK (1979) Landslides in Valles Marineris. J Geophys Res 84:8097–8113

Mathieu L, van Wyk de Vries B (2011) The impact of strike–slip, transtensional and transpressional fault zones on volcanoes. Part I: scaled experiments. J Structural Geol. doi:10.1016/j.jsg2011.03.002

Paguican EMR (2012) The structure, morphology, and surface texture of debris avalanche deposits: field and remote sensing mapping and analogue modelling. Dissertation, Université Blaise Pascal, Clermont-Ferrand

Paguican EMR, van Wyk de Vries B, Lagmay AMF (2011) Hummocks in large avalanches: how they form and what they mean. Geophys Res Abstract. Vol. 13, EGU2011-3437

Paguican EMR, van Wyk de Vries B, Lagmay AMF (2012) Volcano-tectonic controls and emplacement kinematics of the Iriga debris avalanches (Philippines). Bull Volcanol 74 (9):2067–2081. doi:10.1007/s00445-012-0652-7

Palmer AB, Alloway BV, Neall VE (1991) Volcanic debris avalanche deposits in New Zealand —lithofacies organization in unconfined wet-avalanche flows. In: Fisher RV, Smith GA (eds) Sedimentation in volcanic settings. SPEM Special Publication 45, pp 89–98

Pouliquen O, Renaut N (1996) Onset of granular flows on an inclined rough surface: dilutancy effects. J Physique II 6:929–935. doi:10.1051/jp2:1996220

Shea T, van Wyk de Vries B (2008) Structural analysis and analogue modeling of the kinematics and dynamics of rockslide avalanches. Geosphere 4(4):657–686. doi:10.1130/GES00131.1

Shea T, van Wyk de Vries B, Pilato (2008) Emplacement mechanism of contrasting debris avalanches at Volcan Mombacho (Nicaragua), provided by structural and facies analysis. Bull Volcanol 70:899–921. doi:10.1007/s00445-007-0177-7

Siebert L (1984) Large volcanic debris avalanches: characteristics of source areas, deposits, and associated eruptions. J Volcanol Geotherm Res 22:163–197

Siebert L, Beget JE, Glicken H (1995) The 1883 and late prehistoric eruptions of Augustine volcano, Alaska. In: Ida Y, Voight B (eds) Models of magmatic processes and volcanic eruptions. J Volcanol Geotherm Res 66, pp 367-395

Sousa J, Voight B (1995) Multiple-pulsed debris avalanche emplacement at Mount St. Helens in 1980: evidence from numerical continuum flow simulations. J Volcanol Geotherm Res 66:227–250

Staron L, Vilotte JP, Radjai F (2001) Friction and mobilization of contacts in granular numerical avalanches. In: Kishino Y (ed) Powders and grains. Swets and Zeitlinger, Lisse, pp 451–454

Takarada S, Ui T, Yamamoto Y (1999) Depositional features and transportation mechanism of valley-filling Iwasegawa and Kaida debris avalanches, Japan. Bull Volcanol 60:508–522

Thompson N, Bennet MR, Petford N (2010) Development of characteristic volcanic debris avalanche deposit structures: new insights from distinct element simulations. J Volcanol Geotherm Res 192:191–200. doi:10.1016/j.volgeores.2010.02.021

Ui T (1983) Volcanic dry avalanche deposits—identification and comparison with non-volcanic debris stream deposits. J Volcanol Geotherm Res 18:135–150

Ui T, Glicken H (1986) Internal structural variations in a debris-avalanche deposit from ancestral Mount Shasta, California, USA. Bull Volcanol 48:189–194

van Wyk de Vries B, Francis PW (1997) Catastrophic collapse at stratovolcanoes induced by gradual volcano spreading. Nature 387:387–390

van Wyk de Vries B, Kerle N, Petley D (2000) Sector collapse forming at Casita volcano, Nicaragua. Geology 28:167–170

van Wyk de Vries B, Self S, Francis PW, Keszthelyi L (2001) A gravitational spreading origin for the Socompa debris avalanche. J Volcanol Geotherm Res 105:225–227

Vidal N, Merle O (2000) Reactivation of basement faults beneath volcanoes: a new model of flank collapse. J Volcanol Geotherm Res 99:9–26

Voight B, Glicken H, Janda RJ, Douglas PM (1981) Catastrophic rockslide avalanche of May 18. In: Lipman PW, Mullineaux DR (eds) The 1980 eruptions of Mount St. Helens, Washington. US Geol Surv Prof Pap 1250:347-377

Voight B, Glicken H, Janda RJ, Douglass PM (1983) Nature and mechanics of the Mount St Helens rockslide-avalanche of 18 May 1980. Geotechnique 33:243–273

Wadge G, Francis PW, Ramirez CF (1995) The Socompa collapse and avalanche event. In: Ida Y, Voight B (eds) Models of magmatic processes and volcanic eruptions. J Volcanol Geotherm Res 66, pp 309-336

Williams DL, Abrams G, Finn C, Dzurisin D, Johnson DJ, Denlinger R (1987) Evidence from gravity data for an intrusive complex beneath Mount St. Helens. J Geophys Res 92:10207–10222

Wooller L, van Wyk de Vries B, Murray JB, Rymer H, Meyer S (2004) Volcano spreading controlled by dipping substrata. Geology 32(7):573–576. doi:/10.1130/G20472.1

Yoshida H, Sugai T, Ohmori H (2012) Size–distance relationships for hummocks on volcanic rockslide-debris avalanche deposits in Japan. Geomorphology 136(1):76–87. doi:10.1016/j.geomorph.2011.04.044, ISSN 0169-555X

Electronic supplementary material The online version of this article (doi:10.1007/s10346-012-0368-y) contains supplementary material, which is available to authorized users.

E. M. R. Paguican (✉) · B. van Wyk de Vries
Laboratoire Magmas et Volcans, Université Blaise Pascal,
Clermont Université,
5 rue Kessler, 63038, BP 10448, 63000 Clermont-Ferrand, France
e-mail: engiellepaguican@gmail.com

E. M. R. Paguican · B. van Wyk de Vries
UMR 6524, LMV,
CNRS,
63038 Clermont-Ferrand, France

E. M. R. Paguican · B. van Wyk de Vries
R 163, LMV,
IRD,
63038 Clermont-Ferrand, France

E. M. R. Paguican · B. van Wyk de Vries · A. M. F. Lagmay
National Institute of Geological Sciences, College of Science,
University of the Philippines,
Diliman, Quezon 1101, Philippines